



Beaming Effect in Fermi Blazars

W. X. Yang^{1,2,3}, H. G. Wang^{1,2,3}, Y. Liu^{1,2,3}, J. H. Yang⁴ , H. B. Xiao⁵, X. H. Ye^{1,2,3}, Z. Y. Pei^{1,2,3}, L. X. Zhang^{1,2,3} , and J. H. Fan^{1,2,3} 

¹Center for Astrophysics, Guangzhou University, Guangzhou 510006, People's Republic of China; hgwang@gzhu.edu.cn, fjh@gzhu.edu.cn

²Astronomy Science and Technology Research Laboratory of Department of Education of Guangdong Province, Guangzhou 510006, People's Republic of China

³Key Laboratory for Astronomical Observation and Technology of Guangzhou, Guangzhou 510006, People's Republic of China

⁴Department of Physics and Electronics Science, Hunan University of Arts and Science, Changde 415000, People's Republic of China

⁵Shanghai Key Lab for Astrophysics, Shanghai Normal University Shanghai, 200234, People's Republic of China

Received 2021 July 6; revised 2021 November 8; accepted 2021 November 10; published 2022 January 31

Abstract

Blazars show extreme observational properties that are due to the beaming effect with the jet being close to the line of sight. It was found that the observed luminosity is anticorrelated with the synchrotron peak frequency but the debeamed luminosity and the frequency is positively correlated. In this work, we revisit this correlation for a large sample of 255 blazars from the fourth Fermi catalog with available Doppler factors. Our analysis comes to the following conclusions. (1) The observed radio, X-ray, γ -ray, and synchrotron peak luminosity are all anticorrelated with the peak frequency, but the debeamed luminosity is positively correlated with the debeamed peak frequency. The anticorrelation is due to a selection effect or a beaming effect. (2) The Compton dominance parameter is correlated with both the bolometric luminosity and Doppler factor, implying that the more highly Compton-dominated sources are more luminous. (3) The bolometric luminosity can be represented by the γ -ray luminosity for Fermi blazars.

Unified Astronomy Thesaurus concepts: Active galactic nuclei (16); Blazars (164)

Supporting material: machine-readable table

1. Introduction

Blazars show extreme observational properties, such as rapid variability, high and variable polarization, strong emission line features or lack of features, strong γ -ray emission, or superluminal motion (Angel & Stockman 1980; Bassani et al. 1983; Wills et al. 1992; Vermeulen et al. 1994; Urry & Padovani 1995; Hartman et al. 1999; Aller et al. 2011; Ghisellini et al. 2014; Acero et al. 2015; Raiteri et al. 2017; Fan et al. 2016, 2021; Yan et al. 2018; Lu et al. 2019; Yang et al. 2019; Xiao et al. 2019, 2020; Abdollahi et al. 2020; Ajello et al. 2020; Gupta 2020; Pei et al. 2020a, 2020b; Zhang et al. 2020; Zheng et al. 2020; Tripathi et al. 2021; Ye & Fan 2021, and references therein). The extreme observational properties of blazars are due to the beaming effect with the jets pointing close to the line of sight of the observer. In a relativistic beaming model, the observed flux density (f^{ob}) is strongly boosted from the intrinsic one (f^{in}) as $f^{\text{ob}} = \delta^p f^{\text{in}}$, where δ is a Doppler factor (or boosting factor), $p = 2 + \alpha$ for a continuous jet, $p = 3 + \alpha$ for a spherical one, and α is the spectral index ($f_\nu \propto \nu^{-\alpha}$). The frequency follows $\nu^{\text{ob}} = \frac{\delta}{1+z} \nu^{\text{in}}$, where z is the redshift, ν^{ob} is the frequency in the observer frame, and ν^{in} is the frequency in the comoving frame.

Blazars have two main subclasses: BL Lacertae (BL Lac) objects and flat spectrum radio quasars (FSRQs) based on their emission lines features, with BL Lac objects showing weak emission lines or no emission lines at all and FSRQs having strong emission lines. Fan et al. (2016) calculated the spectral energy distributions (SEDs) for a sample of 1492 Fermi Large Area Telescope (LAT) blazars, adopted a Bayesian method for

the distribution of the logarithm of synchrotron peak frequencies, found that three components are the best to fit the distribution, and proposed classifications using the acronyms defined in Abdo et al. (2010): low-synchrotron-peaked blazars (LSPs) if $\log \nu_p(\text{Hz}) \leq 14$, intermediate-synchrotron-peaked blazars (ISPs) if $14.0 < \log \nu_p(\text{Hz}) \leq 15.3$, and high-synchrotron-peaked blazars (HSPs) if $\log \nu_p(\text{Hz}) > 15.3$.

As the next generation instrument after Energetic Gamma Ray Experiment Telescope (Hartman et al. 1999), Fermi/LAT detected a lot of γ -ray emitters. The fourth Fermi/LAT catalog (4FGL) contains 5099 sources (Abdollahi et al. 2020; Ajello et al. 2020). Out of them, 1102 are BL Lac objects, and 681 are FSRQs. There are also many blazar candidates of uncertain type (BCUs).

Many lines of evidence show that γ -rays are strongly beamed. There is a close correlation between γ -rays and radio bands (Dondi & Ghisellini 1995; Fan et al. 1998, 2016; Giroletti et al. 2012), that is, the radio polarization is higher when blazars were detected in the γ -ray bands (Hovatta et al. 2010), and γ -ray luminosity is closely correlated with the Doppler factor (Fan et al. 2013b; Pei et al. 2020a). Superluminal motion, which is one of the observational properties of blazars, has been extensively studied (Zensus et al. 1987; Vermeulen et al. 1994; Kellermann et al. 2004; Lister & Homan 2005; Lister et al. 2009, 2019; Homan et al. 2009); it is found that sources in the Fermi/LAT catalog display higher apparent speeds than those that have not been detected (Piner et al. 2012; Lister et al. 2016; Xiao et al. 2019). Lister et al. (2015) found that the nondetected active galactic nuclei (AGNs) from the 3FGL catalog have significantly lower apparent jet speeds indicating that they have lower than average Doppler factors. From a recent work, it was proposed that the superluminal sources are all γ -ray emitters (Xiao et al. 2020).



Original content from this work may be used under the terms of the [Creative Commons Attribution 4.0 licence](https://creativecommons.org/licenses/by/4.0/). Any further distribution of this work must maintain attribution to the author(s) and the title of the work, journal citation and DOI.

Table 1
Sample of Fermi blazars with Doppler Factors

4FGL name (1)	Other name (2)	redshift (3)	Class (4)	$\log \nu_p$ (5)	$\log L_p$ (6)	$\log L_{\text{syn}}$ (7)	$\log L_R$ (8)	$\log L_O$ (9)	$\log L_X$ (10)	$\log L_\gamma$ (11)	$\log L_{\text{bol}}$ (12)	δ_R (13)
4FGL J0005.9 + 3824	S4 0003 + 38	0.229	FSRQ	14.03	44.653	45.075	41.976	44.37	43.445	45.154	45.417	5.23
4FGL J0016.2-0016	S3 0013-00	1.577	FSRQ	13.58	45.441	46.091	43.963	45.496	45.019	46.760	46.845	18.94
4FGL J0017.5-0514	PMN J0017-0512	0.227	FSRQ	14.48	44.634	45.019	41.462	44.215	43.933	45.518	45.638	12.02
4FGL J0023.7 + 4457	B3 0020 + 446	1.062	FSRQ	12.78	44.726	45.151	42.744	44.243		46.891	46.899	19.63
4FGL J0042.2 + 2319	PKS 0039 + 230	1.426	FSRQ	13.11	45.77	46.192	43.949	45.482		47.138	47.185	13.63
4FGL J0049.7 + 0237	PKS 0047 + 023	1.44	BL Lac	13.48	45.984	46.33	43.482	45.856		47.787	47.802	12.83
...
...
...
...

Notes. Column (1): 4FGL name; Column (2): Other name; Column (3): redshift; Column (4): classification; Column (5): synchrotron peak frequency, $\log \nu_p$ (Hz); Column (6): synchrotron peak luminosity, $\log L_p$ (erg/s); Column (7): integral synchrotron luminosity, $\log L_{\text{syn}}$ (erg/s); Column (8): radio luminosity at 1.4 GHz, $\log L_R$ (erg/s); Column (9): optical luminosity at the R band, $\log L_O$ (erg/s); Column (10): X-ray luminosity, $\log L_X$ (erg/s); Column (11): γ -ray luminosity, $\log L_\gamma$ (erg/s) calculated from the photons and the photon spectral index from Abdollahi et al. (2020); Column (12): bolometric luminosity, $\log L_{\text{bol}}$ (erg/s); Column (13): Doppler factor, δ_R from Liodakis et al. (2018). Only a portion of this table is shown here to demonstrate its form and content. A machine-readable version of the full table is available.

(This table is available in its entirety in a machine-readable form.)

Doppler factors are important for blazars and difficult to be obtained directly, and they have been estimated in the literature (Ghisellini et al. 1993; Mattox et al. 1993; von Montigny et al. 1995; Fan et al. 1999, 2009, 2013a, 2014; Lähteenmäki & Valtaoja 1999; Hovatta et al. 2009; Lister et al. 2009; Savolainen et al. 2010; Liodakis et al. 2018; Pei et al. 2020b; Zhang et al. 2020; Ye & Fan 2021, and references therein). In 1998, Fossati et al. found that there is an anticorrelation between the peak luminosity (and radio luminosity) and the peak frequency for blazars. The luminosity decreases with the synchrotron peak frequency for blazars. Fan et al. (2017) investigated a sample of 86 sources with available Doppler factors and radio, optical, X-ray and γ -ray data and found that there is a real anticorrelation between the luminosity and the synchrotron peak frequency for the observed value; however, there is a positive correlation between the debeamed (intrinsic) luminosity and the frequency. So, they proposed that such a correlation was caused by the beaming effect or selection effect (Fan et al. 2017).

In this work, we will revisit the relationship between the monochromatic luminosity and the peak frequency for both the observed data and debeamed data for a large sample of 255 Fermi blazars with available Doppler factors and redshifts. The sample properties and the results are presented in Section 2. The discussions and conclusions are given in Section 3 and Section 4, respectively.

2. Sample and Results

2.1. Sample

In this work, we compile a sample of 255 blazars (181 FSRQs and 74 BL Lac objects) detected by Fermi/LAT (Abdollahi et al. 2020; Ajello et al. 2020) with available Doppler factors (Liodakis et al. 2018), synchrotron peak frequencies, monochromatic luminosities (radio, optical, X-ray luminosities), synchrotron peak luminosities, and integrated luminosities for the synchrotron bump (Fan et al. 2016; Zhang & Fan 2019). The corresponding data are listed in Table 1.

2.2. Results

2.2.1. Calculations

The γ -ray luminosity can be calculated from the detected photons (see Fan et al. 2012, 2013b; Yang et al. 2017),

$$L_\gamma = 4\pi d_L^2 (1+z)^{(\alpha_\gamma-1)} F,$$

where d_L is the luminosity distance, z is the redshift, α_γ is a γ -ray spectral index, $\alpha_\gamma = \alpha_{\text{ph}} - 1$, α_{ph} is the photon spectral index, and F is the integral flux in units of $\text{GeV cm}^{-2} \text{s}^{-1}$. F can be expressed as

$$F = N_{(E_L \sim E_U)} \left(\frac{1}{E_L} - \frac{1}{E_U} \right) \ln \frac{E_U}{E_L}, \text{ if } \alpha_{\text{ph}} = 2, \text{ otherwise}$$

$$F = N_{(E_L \sim E_U)} \left(\frac{1 - \alpha_{\text{ph}}}{2 - \alpha_{\text{ph}}} \right) \left(\frac{E_U^{2-\alpha_{\text{ph}}} - E_L^{2-\alpha_{\text{ph}}}}{E_U^{1-\alpha_{\text{ph}}} - E_L^{1-\alpha_{\text{ph}}}} \right),$$

where $N_{(E_L \sim E_U)}$ is the total number of photons in the energy range of E_L and E_U . In this work, E_L and E_U correspond to 1 GeV and 100 GeV, respectively.

From the beaming model, the debeamed (intrinsic) luminosity (L_ν^{in}) and frequency ν^{in} can be obtained from the observed luminosity (L_ν^{ob}) and frequency ν^{ob} (Fan et al. 2017)

$$L_\nu^{\text{in}} = L_\nu^{\text{ob}} / \delta^{4+\alpha_\nu}, \quad \nu^{\text{in}} = \nu^{\text{ob}} / \left(\frac{\delta}{1+z} \right),$$

where δ is the Doppler factor, and α_ν ($f_\nu \propto \nu^{-\alpha_\nu}$) is the spectral index at the corresponding band. $\alpha_R = 0$, $\alpha_O = 1.0$ for BL Lac objects, and $\alpha_O = 0.5$ for FSRQs are adopted for the radio and optical spectral indexes, as in Donato et al. (2001) and Abdo et al. (2010). The X-ray spectral indexes, α_X , are considered as in the paper by Fan et al. (2016). An average value is adopted for the unknown α_X , namely, $\langle \alpha_X \rangle = 1.30$ for BL Lac objects and $\langle \alpha_X \rangle = 0.78$ for FSRQs are adopted for the sources without known X-ray spectral indexes. An average value of the redshift, $\langle z \rangle = 0.856$, for BL Lac objects is adopted for two sources (J0532.0-4827 and J1219.0-4827) without known redshifts. The γ -ray spectral index is obtained by

Table 2
Average Values of Luminosity

Para. (1)	Class (2)	Ave. (3)	σ (4)	N (5)	Median (6)	d_{Max} (7)	p (8)
$\log L_{\text{R}}^{\text{ob}}$	BL	42.27	1.05	74	42.34	0.46	2.27×10^{-10}
	FSRQ	43.30	0.66	181	43.40		
$\log L_{\text{O}}^{\text{ob}}$	BL	45.27	0.77	73	45.38	0.23	7.07×10^{-3}
	FSRQ	45.58	0.62	181	45.59		
$\log L_{\text{X}}^{\text{ob}}$	BL	44.19	0.93	52	44.93	0.48	2.67×10^{-8}
	FSRQ	45.04	0.63	129	45.38		
$\log L_{\gamma}^{\text{ob}}$	BL	46.71	0.91	74	46.65	0.31	5.97×10^{-5}
	FSRQ	47.13	0.77	181	47.17		
$\log L_{\text{syn}}^{\text{ob}}$	BL	45.62	0.83	74	45.73	0.33	1.74×10^{-5}
	FSRQ	46.18	0.56	181	46.27		
$\log L_{\text{p}}^{\text{ob}}$	BL	45.22	0.82	74	45.28	0.32	2.37×10^{-5}
	FSRQ	45.81	0.57	181	45.92		
$\log L_{\text{R}}^{\text{in}}$	BL	38.75	1.38	74	38.86	0.14	23%
	FSRQ	38.62	1.43	181	38.42		
$\log L_{\text{O}}^{\text{in}}$	BL	40.94	2.27	73	40.73	0.29	3.0×10^{-4}
	FSRQ	39.73	1.68	181	39.41		
$\log L_{\text{X}}^{\text{in}}$	BL	40.00	2.09	52	40.93	0.15	32%
	FSRQ	39.54	1.77	129	40.20		
$\log L_{\gamma}^{\text{in}}$	BL	42.14	2.07	74	41.86	0.34	7.12×10^{-6}
	FSRQ	40.78	1.75	181	40.55		
$\log L_{\text{syn}}^{\text{in}}$	BL	41.25	1.91	74	41.06	0.27	7.67×10^{-4}
	FSRQ	40.33	1.69	181	39.92		
$\log L_{\text{p}}^{\text{in}}$	BL	40.85	1.92	74	40.62	0.27	6.38×10^{-4}
	FSRQ	39.96	1.65	181	39.58		

Notes. Column information is as follows. Column (1): parameter, where L_i^{ob} denotes for the observed monochromatic luminosity at the i ($i = \text{R}$ (radio), O (optical), X (X-ray), and γ -ray) bands, L_{p} is the peak luminosity, L_{syn} is the integrated synchrotron luminosity, L_i^{in} denotes the intrinsic luminosity at the i band; Column (2): classification; Column (3): averaged logarithmic value of luminosity; Column (4): 1σ uncertainty; Column (5): sample size; Column (6): median value of the logarithm of monochromatic luminosity; Column (7): maximum difference of the two cumulative distribution (d_{Max}); Column (8): probability for the corresponding two distributions to be from the same parent distribution (p).

$\alpha_{\gamma} = \alpha_{\text{ph}} - 1$, where α_{ph} is the photon spectral index from the 4FGL catalog (see Abdollahi et al. 2020; Ajello et al. 2020). The Doppler factor (δ) compiled in this work is from Liodakis et al. (2018); δ ranges from $\delta = 0.22$ for BL Lac object J1725.0 + 1152 to $\delta = 88.44$ for FSRQ J0449.0 + 1121.

2.2.2. Averaged Luminosity

From our calculation of the γ -ray luminosity and the other available luminosities (radio, optical, and X-ray luminosities, synchrotron peak frequency luminosity, and integrated synchrotron bump luminosity) from the papers by Fan et al. (2016) and Zhang & Fan (2019), we can obtain the statistically averaged values. When the Doppler factor (Liodakis et al. 2018) is adopted to the luminosity, the debeamed (intrinsic) monochromatic luminosity, debeamed synchrotron peak frequency luminosity, and debeamed integrated synchrotron bump luminosity can be obtained. For those observed and debeamed data, we calculate their average values for the whole sample,

for BL Lac objects and FSRQs, and obtain the following statistical results. The corresponding average values are listed in Table 2, and the cumulative probabilities are shown in Figures 1 and 2.

The γ -ray luminosity ranges from $\log L_{\gamma}(\text{erg/s}) = 44.43$ (BL J1640.9+1142) to $\log L_{\gamma}(\text{erg/s}) = 49.09$ (FSRQ J1504.4+1029) for the whole sample.

When we consider BL Lac objects and FSRQs separately, we find that, for 75 BL Lac objects, $\log L_{\gamma}(\text{erg/s})$ ranges from $\log L_{\gamma}(\text{erg/s}) = 44.43$ for J1640.9 + 1142 to $\log L_{\gamma}(\text{erg/s}) = 48.31$ for J1248.2 + 5820. The average value is $\langle \log L_{\gamma}(\text{erg/s}) \rangle = 46.71 \pm 0.91$. We also computed their averaged monochromatic radio luminosity $\langle \log L_{\text{R}}(\text{erg/s}) \rangle = 42.27 \pm 1.05$, optical luminosity $\langle \log L_{\text{O}}(\text{erg/s}) \rangle = 45.27 \pm 0.77$ ($N = 73$), X-ray luminosity $\langle \log L_{\text{X}}(\text{erg/s}) \rangle = 44.19 \pm 0.93$ ($N = 52$), synchrotron peak luminosity $\langle \log L_{\text{p}}(\text{erg/s}) \rangle = 45.22 \pm 0.82$, and integrated synchrotron bump luminosity $\langle \log L_{\text{syn}}(\text{erg/s}) \rangle = 45.62 \pm 0.83$.

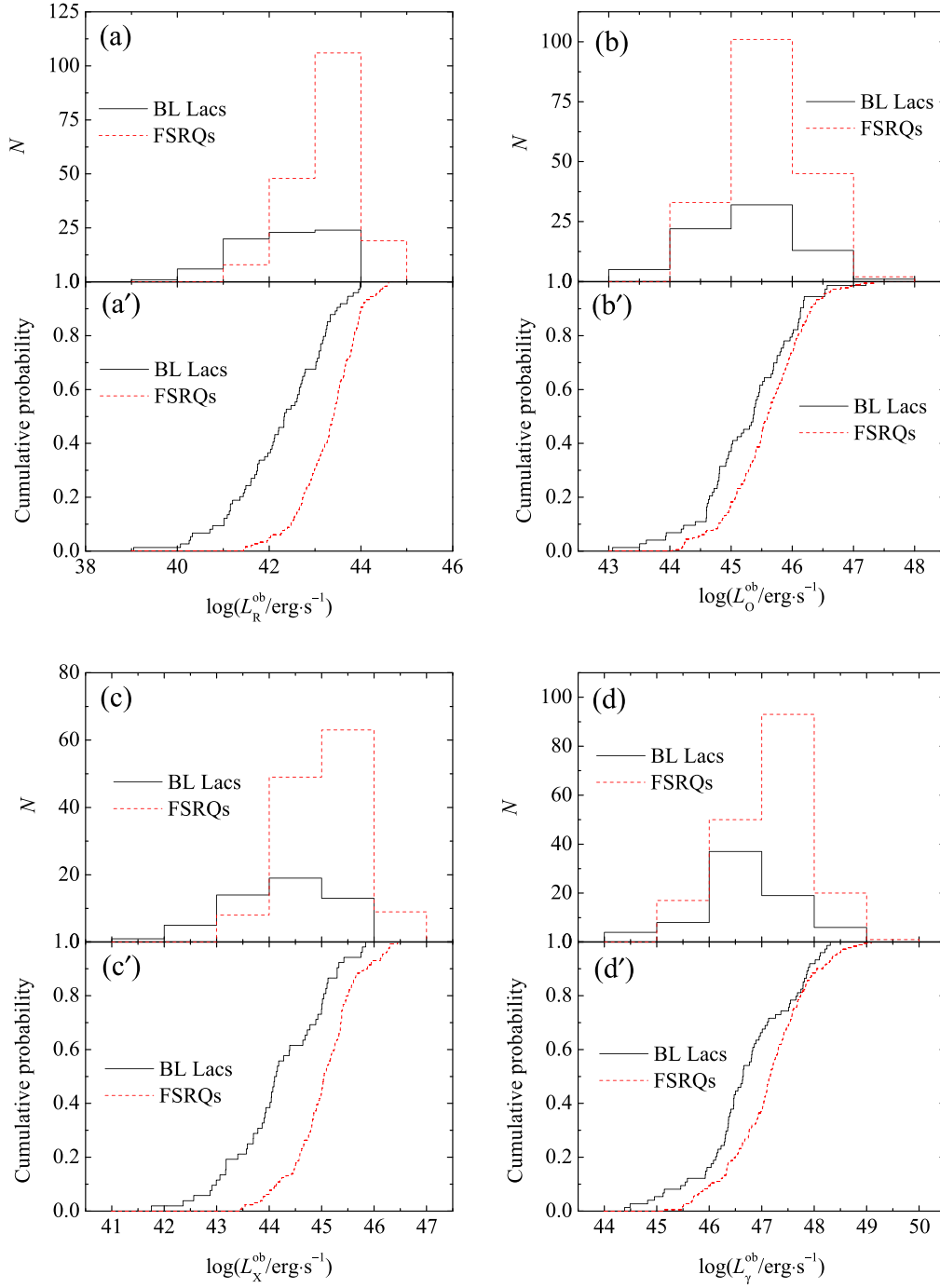


Figure 1. Monochromatic luminosity distribution and corresponding cumulative probability. (a) shows the radio luminosity distribution of BL Lac objects (solid line) and FSRQs (dashed line); (a') shows the cumulative probability of the radio luminosity between BL Lac objects (solid line) and FSRQs (dashed line); (b) and (b') show the optical luminosity; (c) and (c') show the X-ray luminosity; (d) and (d') show the γ -ray luminosity.

For the 181 FSRQs, we find $\log L_\gamma(\text{erg/s})$ to range from $\log L_\gamma(\text{erg/s}) = 45.15$ for J0006.4 + 3825 to $\log L_\gamma(\text{erg/s}) = 49.09$ (FSRQ J1504.4+1029) with an average value of $\langle \log L_\gamma(\text{erg/s}) \rangle = 47.13 \pm 0.77$. The other average values are: radio luminosity $\langle \log L_R(\text{erg/s}) \rangle = 43.30 \pm 0.66$, optical luminosity $\langle \log L_O(\text{erg/s}) \rangle = 45.58 \pm 0.61$, X-ray luminosity $\langle \log L_X(\text{erg/s}) \rangle = 45.04 \pm 0.62$ ($N=129$), synchrotron peak luminosity $\langle \log L_p(\text{erg/s}) \rangle = 45.79 \pm 0.62$, and integrated synchrotron bump luminosity $\langle \log L_{\text{syn}}(\text{erg/s}) \rangle = 46.18 \pm 0.60$.

For the debeamed (intrinsic) luminosity, we have $\langle \log L_R^{\text{in}}(\text{erg/s}) \rangle = 38.75 \pm 1.38$, $\langle \log L_O^{\text{in}}(\text{erg/s}) \rangle = 40.94 \pm 2.27$ ($N=73$), $\langle \log L_X^{\text{in}}(\text{erg/s}) \rangle = 40.00 \pm 2.09$ ($N=52$), and $\langle \log L_\gamma^{\text{in}}(\text{erg/s}) \rangle = 42.16 \pm 2.07$ for BL Lac objects; and $\langle \log L_R^{\text{in}}(\text{erg/s}) \rangle = 38.62 \pm 1.43$, $\langle \log L_O^{\text{in}}(\text{erg/s}) \rangle = 39.73 \pm 1.68$, $\langle \log L_X^{\text{in}}(\text{erg/s}) \rangle = 39.96 \pm 0.62$ ($N=129$), and $\langle \log L_\gamma^{\text{in}}(\text{erg/s}) \rangle = 40.78 \pm 1.75$ for FSRQs.

We can see that the observed luminosity of FSRQs is higher than that of BL Lac objects, but the debeamed luminosity

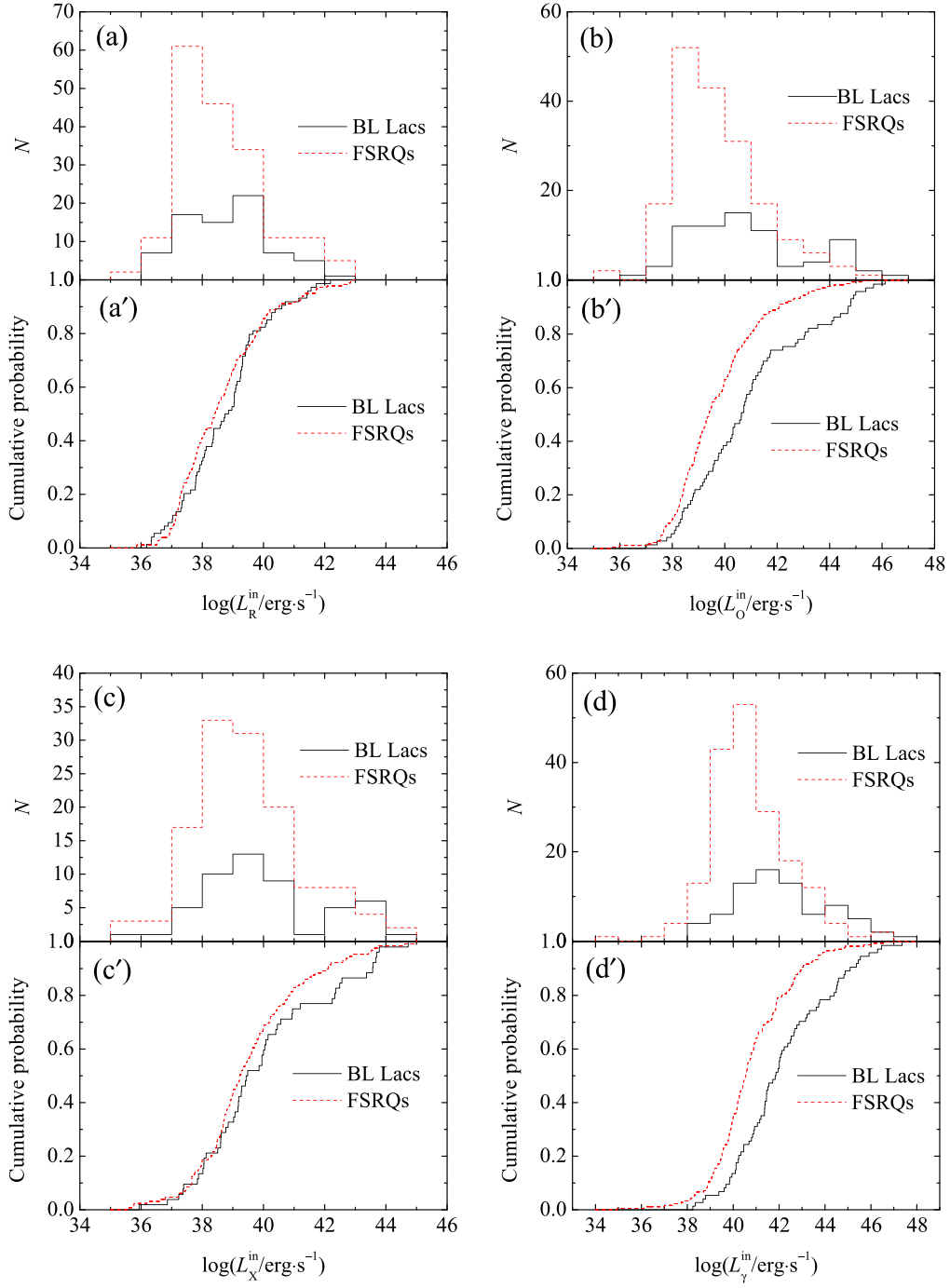


Figure 2. Intrinsic monochromatic luminosity distribution and corresponding cumulative probability. (a) shows the intrinsic radio luminosity distribution of BL Lac objects (solid line) and FSRQs (dashed line); (a') shows the cumulative probability of the intrinsic radio luminosity between BL Lac objects (solid line) and FSRQs (dashed line); (b) and (b') show the optical luminosity; (c) and (c') show the X-ray luminosity; (d) and (d') show the γ -ray luminosity.

(at the optical and γ -ray bands) of FSRQs is lower than that of BL Lac objects. When a Kolmogorov–Smirnov test (K–S test) is applied to the observed and debeamed (intrinsic) luminosities, it is found that the probabilities for the distributions of the observed monochromatic luminosity, synchrotron peak luminosity, and integrated synchrotron bump luminosity of FSRQs and those of BL Lac objects to be from the same distribution are all smaller than 7.07×10^{-3} , implying that the difference in the observed luminosity between BL Lac objects and FSRQs is significant. The probability for the distributions of the debeamed monochromatic optical luminosity, γ -ray luminosity,

synchrotron peak luminosity, and integrated synchrotron bump luminosity of FSRQs and those of BL Lac objects to be from the same distribution are all smaller than 7.67×10^{-4} , suggesting that those differences are significant. However, the probability for the distributions of the debeamed radio luminosity and optical luminosity of FSRQs and those of BL Lac objects are 23% and 32%, respectively. This means that there is no clear difference in the debeamed radio luminosity or optical luminosity between BL Lac objects and FSRQs. The K–S test results are shown in Figure 1 for the observed luminosity and Figure 2 for the debeamed luminosity.

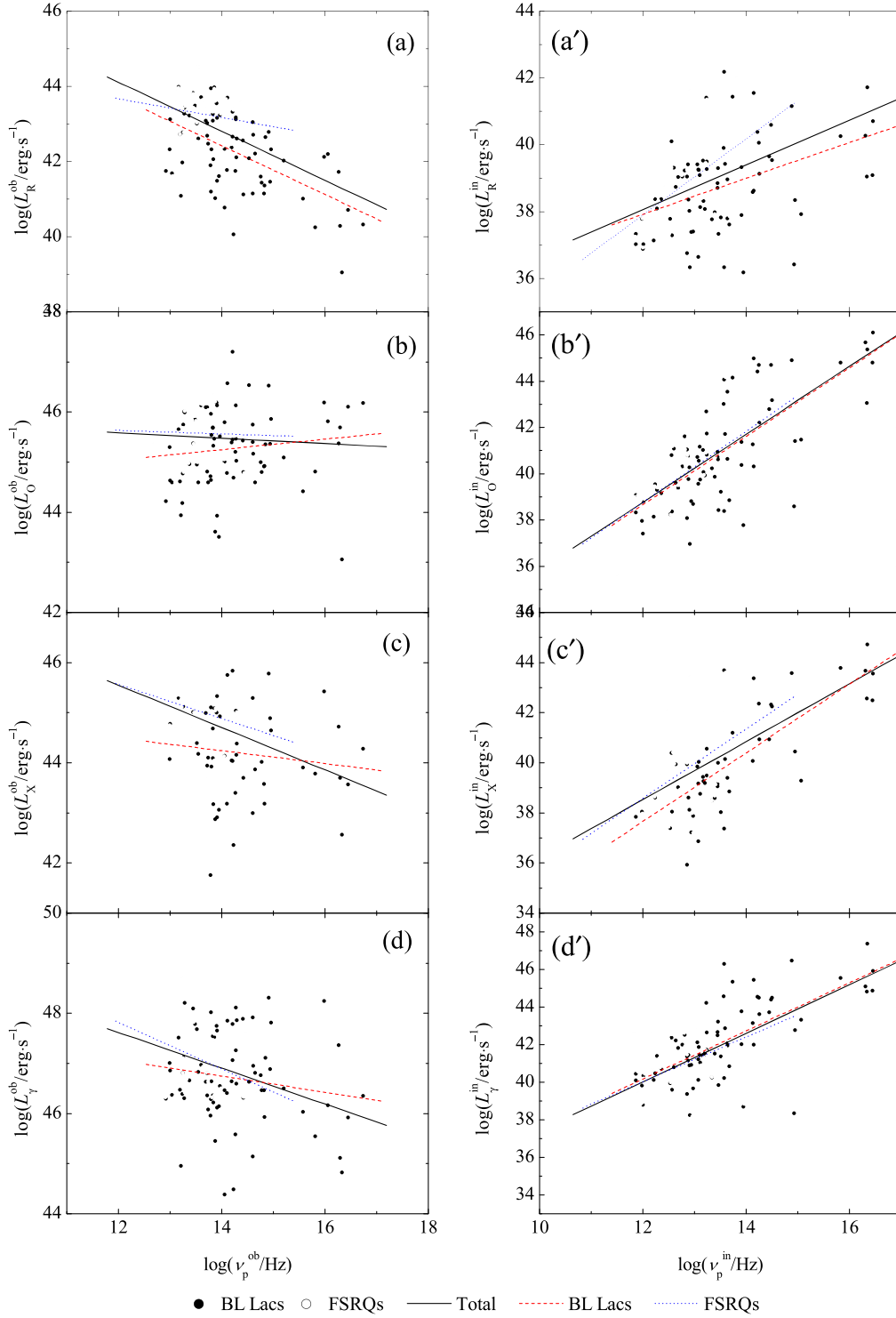


Figure 3. Correlation between luminosity ($\log L_\nu$) and peak frequency ($\log \nu_p$). (a) shows $\log L_R^{\text{ob}}$ and $\log \nu_p^{\text{ob}}$; (a') presents the corresponding intrinsic data ($\log L_R^{\text{in}}$ and $\log \nu_p^{\text{in}}$); (b) and (b'), (c) and (c'), and (d) and (d') show the optical (X-ray, and γ -ray) luminosities and peak frequencies.

2.2.3. Correlation between Luminosity and Peak Frequency

When a linear regression is applied to the observed and the intrinsic data to investigate the correlation between the luminosity and the synchrotron peak frequency, we derive the following results:

$$\log L_\gamma^{\text{ob}} = -(0.36 \pm 0.07) \log \nu_p^{\text{ob}} + (51.91 \pm 0.91),$$

with a correlation coefficient $r = -0.32$ and a chance probability of $p < 10^{-4}$ for the observed data and

$$\log L_\gamma^{\text{in}} = (1.29 \pm 0.11) \log \nu_p^{\text{in}} + (24.49 \pm 1.39),$$

with $r = 0.602$ and $p < 10^{-4}$ for the intrinsic data. The corresponding results and those for other bands are shown in Figure 3 for the observed data and the intrinsic data. The

Table 3
Linear Correlation Fitting Results, $y = ax + b$

$y \sim x$ (1)	Class (2)	$a \pm \Delta a$ (3)	$b \pm \Delta b$ (4)	N (5)	r (6)	p (7)
$\log L_R^{\text{ob}} \sim \log \nu_p^{\text{ob}}$	T	-0.65 ± 0.07	51.95 ± 0.90	255	-0.532	$< 10^{-4}$
	B	-0.65 ± 0.11	51.52 ± 1.61	74	-0.562	$< 10^{-4}$
	F	-0.25 ± 0.09	46.65 ± 1.20	181	-0.204	5.85×10^{-3}
$\log L_O^{\text{ob}} \sim \log \nu_p^{\text{ob}}$	T	-0.05 ± 0.06	46.22 ± 0.78	254	-0.059	35.15%
	B	0.10 ± 0.10	43.79 ± 1.42	73	0.123	30%
	F	-0.03 ± 0.09	46.04 ± 1.16	181	-0.030	69.17%
$\log L_X^{\text{ob}} \sim \log \nu_p^{\text{ob}}$	T	-0.42 ± 0.07	50.62 ± 1.03	181	-0.390	$< 10^{-4}$
	B	-0.13 ± 0.14	46.03 ± 2.05	52	-0.126	37.4%
	F	-0.34 ± 0.10	49.66 ± 1.40	129	-0.281	1.24×10^{-3}
$\log L_\gamma^{\text{ob}} \sim \log \nu_p^{\text{ob}}$	T	-0.36 ± 0.07	51.91 ± 0.91	255	-0.321	$< 10^{-4}$
	B	-0.16 ± 0.12	49.02 ± 1.66	74	-0.162	16.7%
	F	-0.46 ± 0.10	53.39 ± 1.36	181	-0.326	$< 10^{-4}$
$\log L_p^{\text{ob}} \sim \log \nu_p^{\text{ob}}$	T	-0.33 ± 0.06	50.13 ± 0.79	255	-0.337	$< 10^{-4}$
	B	-0.19 ± 0.10	47.89 ± 1.49	74	-0.206	7.8%
	F	-0.25 ± 0.08	49.13 ± 1.12	181	-0.216	3.45×10^{-3}
$\log L_{\text{syn}}^{\text{ob}} \sim \log \nu_p^{\text{ob}}$	T	-0.27 ± 0.06	49.71 ± 0.80	255	-0.280	$< 10^{-4}$
	B	-0.16 ± 0.11	47.91 ± 1.51	74	-0.176	13.38%
	F	-0.13 ± 0.08	47.87 ± 1.12	181	-0.113	13.15%
$\log L_R^{\text{in}} \sim \log \nu_p^{\text{in}}$	T	0.67 ± 0.09	30.03 ± 1.15	255	0.427	$< 10^{-4}$
	B	0.53 ± 0.13	31.53 ± 1.79	74	0.430	1.3×10^{-4}
	F	1.14 ± 0.14	24.20 ± 1.81	181	0.512	$< 10^{-4}$
$\log L_O^{\text{in}} \sim \log \nu_p^{\text{in}}$	T	1.47 ± 0.10	21.13 ± 1.27	254	0.685	$< 10^{-4}$
	B	1.48 ± 0.16	20.88 ± 2.24	73	0.729	$< 10^{-4}$
	F	1.54 ± 0.16	20.29 ± 2.00	181	0.589	$< 10^{-4}$
$\log L_X^{\text{in}} \sim \log \nu_p^{\text{in}}$	T	1.16 ± 0.12	24.66 ± 1.58	181	0.580	$< 10^{-4}$
	B	1.37 ± 0.16	21.22 ± 2.21	52	0.770	$< 10^{-4}$
	F	1.39 ± 0.22	21.91 ± 2.76	129	0.493	$< 10^{-4}$
$\log L_\gamma^{\text{in}} \sim \log \nu_p^{\text{in}}$	T	1.29 ± 0.11	24.49 ± 1.39	255	0.602	$< 10^{-4}$
	B	1.28 ± 0.16	24.82 ± 2.16	74	0.688	$< 10^{-4}$
	F	1.19 ± 0.18	25.73 ± 2.31	181	0.438	$< 10^{-4}$
$\log L_p^{\text{in}} \sim \log \nu_p^{\text{in}}$	T	1.22 ± 0.10	24.53 ± 1.25	255	0.620	$< 10^{-4}$
	B	1.20 ± 0.15	24.64 ± 1.99	74	0.694	$< 10^{-4}$
	F	1.37 ± 0.16	22.60 ± 2.05	181	0.535	$< 10^{-4}$
$\log L_{\text{syn}}^{\text{in}} \sim \log \nu_p^{\text{in}}$	T	1.28 ± 0.10	24.12 ± 1.25	255	0.640	$< 10^{-4}$
	B	1.21 ± 0.14	24.84 ± 1.94	74	0.706	$< 10^{-4}$
	F	1.50 ± 0.16	21.33 ± 2.04	181	0.571	$< 10^{-4}$
$\delta \sim \log \nu_p^{\text{ob}}$	T	-4.46 ± 0.99	77.87 ± 13.58	255	-0.273	$< 10^{-4}$
	B	-2.46 ± 1.35	46.89 ± 19.25	74	-0.210	7.3%
	F	-4.19 ± 1.68	75.14 ± 22.66	181	-0.183	1.4%
$\log(\text{CDP}) \sim \log L_\gamma^{\text{ob}}$	T	0.41 ± 0.04	-18.10 ± 1.81	255	0.543	$< 10^{-4}$
	B	0.24 ± 0.06	-9.87 ± 2.78	74	0.433	1.15×10^{-4}
	F	0.58 ± 0.05	-26.03 ± 2.15	181	0.656	$< 10^{-4}$
$\log L_{\text{bol}} \sim \log L_\gamma$	T	0.94 ± 0.01	2.94 ± 0.37	255	0.991	$< 10^{-4}$
	B	0.97 ± 0.01	1.29 ± 0.41	74	0.997	$< 10^{-4}$
	F	0.91 ± 0.01	4.50 ± 0.48	181	0.989	$< 10^{-4}$

Table 3
(Continued)

$y \sim x$ (1)	Class (2)	$a \pm \Delta a$ (3)	$b \pm \Delta b$ (4)	N (5)	r (6)	p (7)
$\log(\text{CDP}) \sim \log L_\gamma$	T	0.36 ± 0.04	-15.67 ± 1.94	251	0.487	$<10^{-4}$
	B	0.22 ± 0.06	-8.65 ± 2.93	74	0.377	9.24×10^{-4}
	F	0.54 ± 0.05	-24.11 ± 2.45	177	0.618	$<10^{-4}$
$\log(\text{CDP}) \sim \log \delta$	T	0.39 ± 0.11	0.96 ± 0.12	244	0.228	3.33×10^{-4}
	B	0.12 ± 0.16	1.35 ± 0.16	68	0.096	43.54%
	F	0.70 ± 0.15	0.55 ± 0.18	176	0.341	$<10^{-4}$
$\log L_\gamma^{\text{in}} \sim \log \delta$	T	-4.53 ± 0.15	46.10 ± 0.18	248	-0.882	$<10^{-4}$
	B	-4.07 ± 0.24	45.72 ± 0.25	68	-0.901	$<10^{-4}$
	F	-4.76 ± 0.21	46.36 ± 0.25	180	-0.864	$<10^{-4}$

Notes. Column (1): relation; Column (2): classification, where T stands for the whole sample, B for BL Lac objects, and F for FSRQs; Column (3): slope and corresponding uncertainty ($a \pm \Delta a$); Column (4): intercept and corresponding uncertainty ($b \pm \Delta b$); Column (5): sample size (N); Column (6): correlation coefficient (r); and Column (7): chance probability (p).

figures also clearly indicate that the observed radio (X-ray) luminosity is anticorrelated with the synchrotron peak frequency while the debeamed radio (optical and X-ray) luminosity is positively correlated with the debeamed synchrotron peak frequency. The corresponding correlation results are shown in Table 3, in which Column (1) gives the relation; Column (2) gives the classification, T stands for the whole sample, B stands for BL Lac objects, and F stands for FSRQs; Column (3) shows the slope and the corresponding uncertainty ($a \pm \Delta a$); Column (4) gives the intercept and the corresponding uncertainty ($b \pm \Delta b$); Column (5) is the sample size (N); Column (6) is the correlation coefficient (r); and Column (7) is the chance probability (p).

3. Discussions

The SEDs of blazars consist of two bumps; the lower-energy bump (or synchrotron bump), which is located in the infrared to X-ray, is due to synchrotron emission while the higher-energy bump, which is located from the X-rays through MeV bands, originates from inverse Compton emission. In 1998, Fossati et al. computed the SEDs of a sample of 126 blazars and found that the 5 GHz radio luminosity, synchrotron peak luminosity, and γ -ray luminosity are all anticorrelated with the synchrotron peak frequency and that the luminosity decreases with the peak frequency. The results implies that there is a sequence from FSRQs to XBLs, with luminosity decreasing while the peak frequency increases, known as the blazar sequence. Mao et al. (2016) obtained SEDs for a large sample of Roma-BZCAT blazars and found a similar result with the peak frequency increasing when the radio (and bolometric/integrated synchrotron) luminosity decreases.

However, Giommi et al. (2005) detected luminous high-frequency BL Lac objects and low-frequency low-luminosity BL Lac objects. Later on, the anticorrelation of the observed data was not observed for the intrinsic data (Nieppola et al. 2008). Giommi et al. (2012b) did not find an anticorrelation for an FSRQ sample either. From simulations, Giommi et al. (2012a) found an anticorrelation between the radio luminosity and synchrotron peak frequency and proposed that the anticorrelation is due to a selection effect. Fan et al. (2017) calculated the intrinsic SEDs for a sample of 86 flaring Fermi

blazars and found an anticorrelation between the luminosity (at radio, optical, X-rays, γ -rays, and the synchrotron peak) and the peak frequency for the observed data, but the correlation for intrinsic data is positive. They proposed that the anticorrelation originates from the beaming effect or a selection effect. In that paper, Fan et al. (2017) stated, ‘‘Since our Fermi blazar sample with a known Doppler factor is small, we will try to compute more Doppler factors for the Fermi blazars and redo the analysis in the future.’’ Now, Doppler factors were obtained for a large sample of blazars (Lioudakis et al. 2018), which offers a good opportunity to reanalyze the correlation between the γ -ray luminosity and the peak frequency for both the observed data and the intrinsic data. That is the motivation of this work.

By cross-checking the latest 4FGL catalog (Abdollahi et al. 2020), available Doppler factors (Lioudakis et al. 2018), synchrotron peak frequency (Fan et al. 2016; Zhang & Fan 2019), and redshifts, we revisit the correlation between γ -ray (or radio, optical, X-ray, peak frequency, integrated synchrotron) luminosity and the synchrotron peak frequency and compile a large sample of 260 Fermi blazars. Out of the 260 blazars, five are BCU (J1131.9-0503, J0205.0+1510, J1416.0+1325, J0618.9-1138, and J0357.1+2325), 74 are BL Lac objects, and 181 are FSRQs. In this work, we only consider the 255 identified sources.

Average luminosity. From Table 2, it can be found that the monochromatic luminosity (at the radio, optical, X-ray, and γ -ray bands), the integrated synchrotron luminosity and the synchrotron peak luminosity for FSRQs are higher than those for BL Lac objects, and their difference is clear. The K–S test shows that the probability for the luminosity distribution of BL Lac objects and that of FSRQs to be from the same parent distribution is less than 7.1×10^{-3} .

For the intrinsic luminosity, $L_\nu^{\text{in}} = L_\nu^{\text{ob}} / \delta^{4+\alpha_\nu}$, we can see that the averaged intrinsic monochromatic luminosity of BL Lac objects is higher than that of FSRQs. The probabilities for the distributions of the intrinsic optical and γ -ray luminosities for BL Lac objects and those of FSRQs to be from the same parent distributions are 3×10^{-4} and 7.12×10^{-6} , but the K–S test suggests that the intrinsic radio and X-ray luminosities for both BL Lac objects and FSRQs show similar distributions since the probabilities for the two distributions to be from the same parent distribution are 23% at the radio band and 32% at

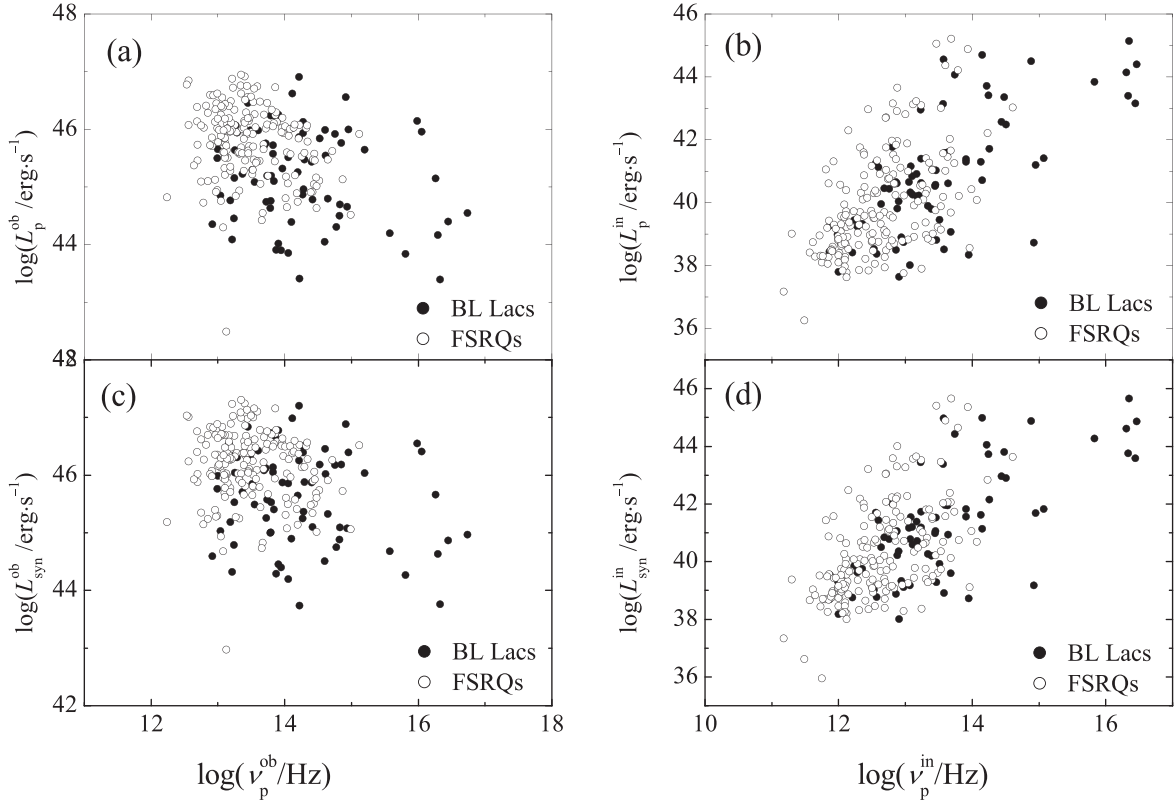


Figure 4. (a) Correlation between observed peak luminosity ($\log L_p^{\text{ob}}$) and observed peak frequency ($\log \nu_p^{\text{ob}}$), where filled circles stand for BL Lac objects and open circles for FSRQs; (b) correlation between intrinsic peak luminosity ($\log L_p^{\text{in}}$) and intrinsic peak frequency ($\log \nu_p^{\text{in}}$); (c) correlation between observed integrated luminosity for the synchrotron bump ($\log L_{\text{syn}}^{\text{ob}}$) and observed peak frequency ($\log \nu_p^{\text{ob}}$); (d) correlation between intrinsic integrated luminosity for the synchrotron bump ($\log L_{\text{syn}}^{\text{in}}$) and intrinsic peak frequency ($\log \nu_p^{\text{in}}$).

the radio and X-ray bands. We conclude that BL Lac objects and FSRQs have the same intrinsic luminosity distributions in the radio band, and their averaged and median luminosities are $\langle \log L_R^{\text{in}} \rangle = 38.75 \pm 1.38$ and $\log L_{\text{Med}}^{\text{in}} = 38.86$ for BL Lac objects and $\langle \log L_R^{\text{in}} \rangle = 38.62 \pm 1.43$ and $\log L_{\text{Med}}^{\text{in}} = 38.42$ for FSRQs. In the X-ray band, we believe that the similar distribution is due to the fact that we used the average X-ray spectral index for the unknown X-ray spectral index when we derive the intrinsic X-ray luminosity. If we only consider the blazars with known X-ray spectral indexes, it is found that the average X-ray luminosities are $\langle \log L_X^{\text{in}} \rangle = 40.42 \pm 2.20$ for BL Lac objects and $\langle \log L_X^{\text{in}} \rangle = 39.5 \pm 1.85$ for FSRQs. The average intrinsic X-ray luminosity in BL Lac objects is higher than that in FSRQs. The K–S test indicates that the probability for the two distributions to be from the same parent distribution is 5.7%. From our analysis, it is found that BL Lac objects and FSRQs have similar intrinsic radio luminosities, but BL Lac objects have higher intrinsic optical, X-ray, and γ -ray luminosities than FSRQs.

Luminosity–peak frequency correlation. The present work gives a close anticorrelation between the γ -ray luminosity and synchrotron peak frequency for the whole blazar sample: $\log L_\gamma^{\text{ob}} = -(0.36 \pm 0.07) \log \nu_p^{\text{ob}} + 51.91 \pm 0.91$, with $r = -0.32$ and $p < 10^{-4}$, which is similar to the result $\log L_\gamma^{\text{ob}} = -(0.580 \pm 0.166) \log \nu_p^{\text{ob}} + 53.918 \pm 2.276$, with $r = -0.356$ and $p = 7.73 \times 10^{-4}$ (Fan et al. 2017). When BL Lac objects and FSRQs are considered separately, the following results are obtained: $\log L_\gamma^{\text{ob}} = -(0.16 \pm 0.12) \log \nu_p^{\text{ob}} + 49.02 \pm 1.66$ with $r = -0.16$ and $p = 16.7\%$ for 74 BL

Lac objects and $\log L_\gamma^{\text{ob}} = -(0.46 \pm 0.10) \log \nu_p^{\text{ob}} + 53.39 \pm 1.36$ with $r = -0.33$ and $p < 10^{-4}$ for 181 FSRQs. All the correlation results are listed in Table 3 and shown in Figure 3 and Figure 4.

When we consider the intrinsic data, $\log L_\gamma^{\text{in}} = (1.29 \pm 0.11) \log \nu_p^{\text{in}} + 24.49 \pm 1.39$ with $r = 0.60$ and $p < 10^{-4}$ is obtained for the whole sample. For the two subsamples, we have $\log L_\gamma^{\text{in}} = (1.28 \pm 0.16) \log \nu_p^{\text{in}} + 24.82 \pm 2.16$ with $r = 0.69$ and $p < 10^{-4}$ for the 74 BL Lac objects and $\log L_\gamma^{\text{in}} = (1.19 \pm 0.18) \log \nu_p^{\text{in}} + 25.73 \pm 2.31$ with $r = 0.44$ and $p < 10^{-4}$ for the 181 FSRQs. The corresponding results are shown in Figure 3 and Figure 4 and listed in Table 3. It is clear that there is an anticorrelation between the observed luminosity (at the radio, X-ray, and γ -ray bands) and synchrotron peak frequency, and there is an anticorrelation between the peak luminosity (or integrated synchrotron luminosity) and peak frequency (see Figure 4). Our results about the observed luminosity and peak frequency are consistent with those by Fossati et al. (1998), Niappola et al. (2008), and Mao et al. (2016). In this work, we do not find a correlation for the optical band with the chance probabilities being $p \sim 35\%$, 30%, and 69% for the whole sample, BL Lac objects, and FSRQs, respectively. This is consistent with the result by Fan et al. (2017). This might result from the contributions of the accretion disk emission in FSRQs or host galaxy emission in BL Lac objects. However, there is a close positive correlation between the intrinsic luminosity (at the radio, optical, X-ray, and γ -ray bands; peak frequency; and integrated synchrotron luminosity) and the intrinsic

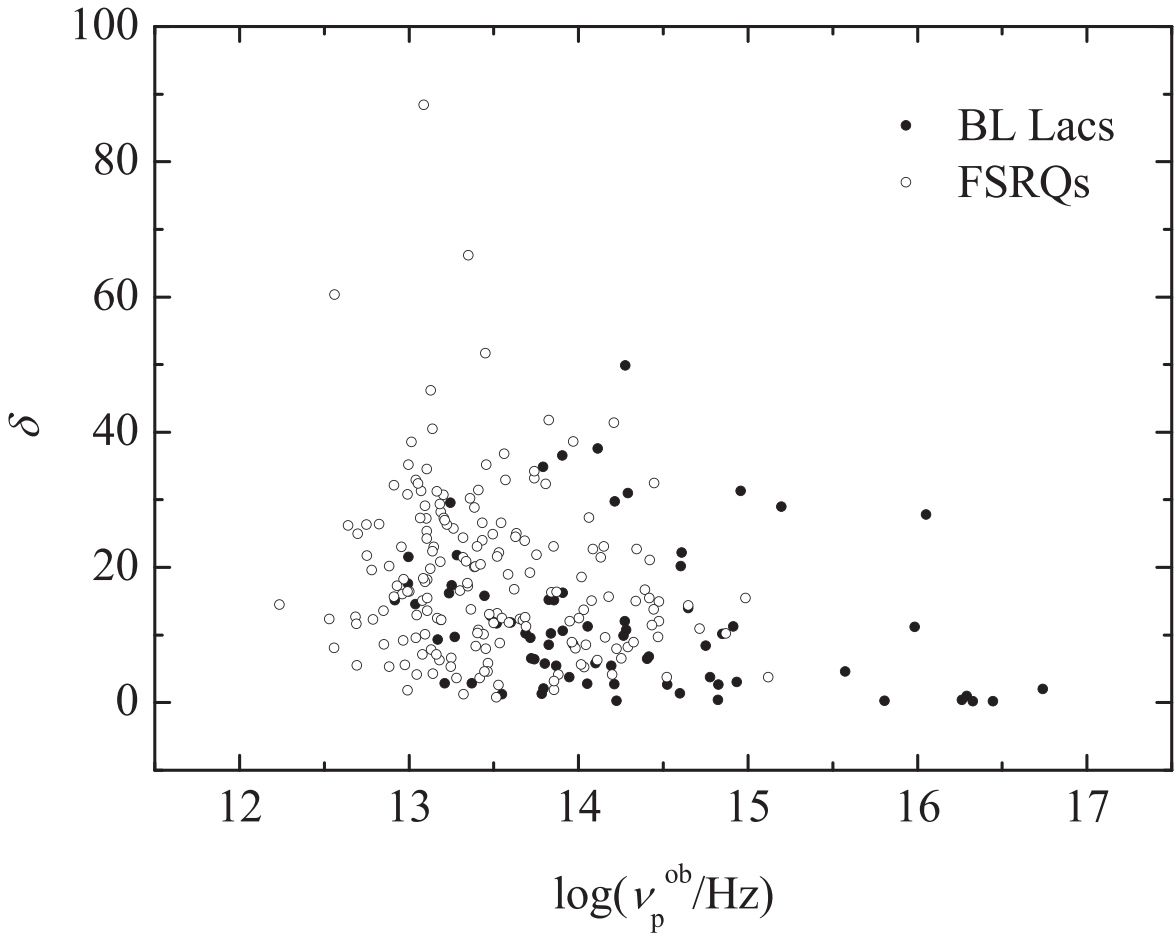


Figure 5. Plot of Doppler factor (δ) against peak frequency, where filled circles stand for BL Lac objects and open circles for FSRQs.

synchrotron peak frequency, as discussed in Nieppola et al. (2008) and Fan et al. (2017).

Doppler factor. The Doppler factor, $\delta = \frac{1}{\Gamma(1 - \beta \cos \theta)}$, is an important physics parameter in AGNs, which depends on two parameters that cannot be directly observed, the bulk velocity, β , which can be expressed using the Lorentz factor as, $\Gamma = \frac{1}{\sqrt{1 - \beta^2}}$, and the viewing angle, θ . So, it is difficult to obtain the Doppler factor directly from observations. Fortunately, some indirect methods have been proposed (Ghisellini et al. 1993; Mattox et al. 1993; Fan et al. 1999, 2009, 2013b; Lähteenmäki & Valtaoja 1999; Hovatta et al. 2009; Liodakis et al. 2018; Pei et al. 2020b; Zhang et al. 2020; Chen et al. 2021; Ye & Fan 2021). However, it is known that there is some difference in the Doppler factors estimated from different methods. Zhang et al. (2020) compared their Doppler factor values with those estimated in the literature (Ghisellini et al. 2014; Chen 2018; Liodakis et al. 2018) for common sources and found that the mean values from different literature are $\langle \delta \rangle = 12.88$ (Ghisellini et al. 2014), $\langle \delta \rangle = 20.0$ (Liodakis et al. 2018), $\langle \delta \rangle = 13.87$ (Chen 2018), and $\langle \delta \rangle = 13.16$ (Zhang et al. 2020) for FSRQs and $\langle \delta \rangle = 12.44$ (Ghisellini et al. 2014), $\langle \delta \rangle = 16.68$ (Liodakis et al. 2018), $\langle \delta \rangle = 27.33$ (Chen 2018), and $\langle \delta \rangle = 10.25$ (Zhang et al. 2020) for BL Lac objects. From the comparison, we can see that the average value of the Doppler factor of FSRQs is higher than that of BL Lac objects in these publications (Ghisellini et al. 2014; Liodakis et al. 2018; Zhang et al. 2020), but there are some differences in the

Doppler factor values estimated using different methods. So, we want to stress that the result pertaining to the intrinsic data depends strongly on the Doppler factors, and this dependence will strongly influence our statistical results. Therefore, it is very important to have a good method for the estimation of the Doppler factor.

In this work, we adopted the Doppler factors from the work by Liodakis et al. (2018), who obtained the Doppler factors from radio variability for more than 800 sources. For the present sample of 255 sources, the Doppler factors range from $\delta = 0.22$ to $\delta = 88.44$. In our considerations, if $\delta < 1.0$, then $\delta = 1$ is adopted when we compute the intrinsic luminosity and peak frequency, namely, $L_\nu^{\text{in}} = L_\nu^{\text{ob}}$ and $\nu_p^{\text{in}} = \nu_p^{\text{ob}}$. The Doppler factor in the work is plotted against the peak frequency in Figure 5, which shows a tendency for the Doppler factor to decrease with the synchrotron peak frequency, as found in Nieppola et al. (2008). So, the lower peak frequency sources have larger Doppler factors and are strongly boosted to become more luminous, $L_\nu^{\text{ob}} = \delta^{4+\alpha} L_\nu^{\text{in}}$, than are the higher peak frequency sources. Such an effect results in an anticorrelation between the luminosity and the peak frequency, as obtained and discussed in the literature (Fossati et al. 1998; Padovani 2007; Nieppola et al. 2008; Ghisellini & Tavecchio 2008). This kind of anticorrelation is caused by a selection effect (Giommi et al. 2012b, 2012a) or a beaming effect (Fan et al. 2017).

Giommi et al. (2012b) stated that an unbiased sample was needed to test the robustness of the the *blazar sequence*, for

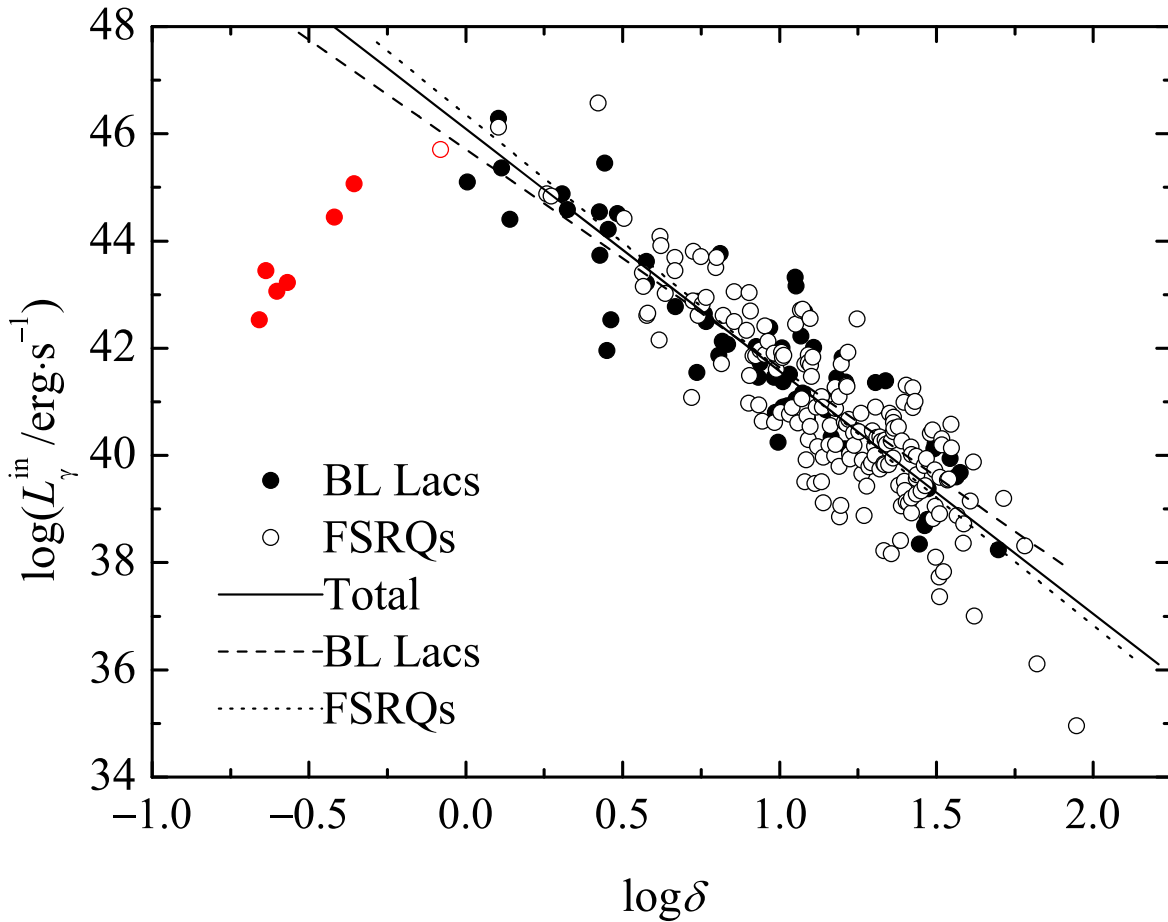


Figure 6. Plot of intrinsic γ -ray luminosity ($\log L_{\gamma}^{\text{in}}$) against Doppler factor (δ), where filled circles stand for BL Lac objects and open circles for FSRQs. The red points stand for the sources with $\delta < 1.0$. The straight lines corresponds to the best-fitting results, the solid line to the whole sample with $\delta > 1.0$, the dashed line to BL Lac objects, and the dotted line to FSRQs.

which there is a strong anticorrelation between the luminosity and the peak frequency (Fossati et al. 1998; Ghisellini et al. 1998), but an unbiased sample is not easy to obtain. As Giommi et al. (2012b) mentioned, their samples were not unbiased even though they were statistically well-defined. They showed that the distribution of the synchrotron peak frequency ($\log \nu_p$) strongly depends on the selection method so that different samplings of the parameter ($\log \nu_p$) are obtained for the various samples. They also noticed that the nonthermal emission of BL Lac objects with higher peak frequencies dominates the emission of their host galaxy, so that they show featureless spectra and only a lower limit on the redshift can be obtained. Bright BL Lac objects with known redshifts and lower peak frequencies may be between BL Lac objects and FSRQs. In this case, one can conclude that bright FSRQs (and some lower-peaked BL Lac objects) have lower frequencies, while higher-peaked BL Lac objects have only lower limits on their luminosity. Therefore, an apparent anticorrelation shows up between the luminosity and peak frequency. Using Monte Carlo simulations, Giommi et al. (2012a) obtained an L-shaped distribution of the luminosity against the synchrotron peak frequency ($\log L$ versus $\log \nu_p$) if blazars with no redshift measurements are not properly taken into account.

Blazars show extreme observational properties, which are due to the beaming effect. Observations also indicate that FSRQs are more luminous than BL Lac objects, and the Doppler factors of BL Lac objects are lower than those of FSRQs. One can expect

that sources with stronger boosting effects are brighter and easier to detect. So, Fan et al. (2017) proposed that the anticorrelation between the luminosity and frequency for the observed data is from the beaming effect and used the intrinsic data to investigate the correlation. They found positive correlations for the intrinsic data and stated that the anticorrelation for the observed data is caused by a beaming effect.

We also investigated the correlation between the Doppler factor ($\log \delta$) and intrinsic γ -ray luminosity ($\log L_{\gamma}^{\text{in}}$) and found that they show an anticorrelation

$$\log L_{\gamma}^{\text{in}} = -(4.53 \pm 0.15) \log \delta + 46.10 \pm 0.18,$$

with $r = -0.882$ and $p < 10^{-4}$ for the whole sample of 248 sources with $\delta > 1.0$. When we considered BL Lac objects and FSRQs separately, it is found that $\log L_{\gamma}^{\text{in}} = -(4.07 \pm 0.24) \log \delta + 45.72 \pm 0.25$ with $r = -0.901$ and $p < 10^{-4}$ for 68 BL Lac objects and $\log L_{\gamma}^{\text{in}} = -(4.76 \pm 0.21) \log \delta + 46.36 \pm 0.25$ with $r = -0.864$ and $p < 10^{-4}$ for 180 FSRQs. The scattering points and the corresponding best-fitting results are shown in Figure 6 and listed in Table 3. Since the beaming model gives $L_{\gamma}^{\text{ob}} = \delta^{4+\alpha_{\gamma}} L_{\gamma}^{\text{in}}$, where $\alpha_{\gamma} = \alpha_{\text{ph}} - 1$, one can estimate the Doppler factor by adopting the obtained linear correlation, namely, $\delta = (4.42 L_{47})^{\frac{1}{\alpha_{\text{ph}} - 1.763}}$ for FSRQs, $\delta = (19.28 L_{47})^{\frac{1}{\alpha_{\text{ph}} - 1.073}}$

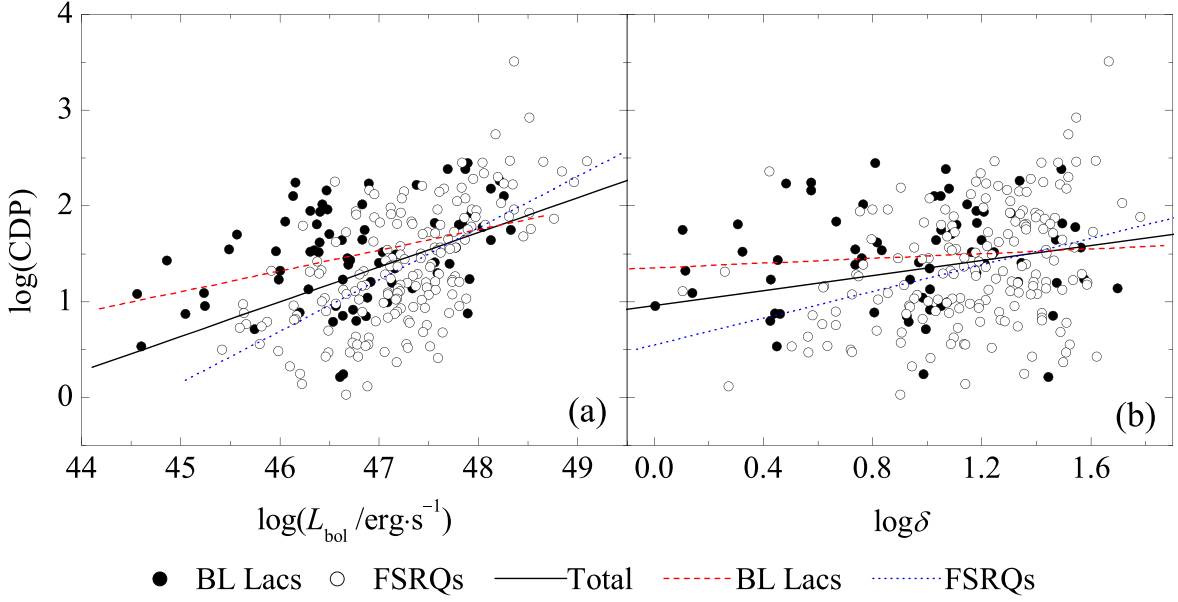


Figure 7. Plot of the Compton dominance parameter against the bolometric luminosity in the left panel. Plot of the Compton dominance parameter against the Doppler factor in the right panel. Filled circles stand for BL Lac objects and open circles for FSRQs.

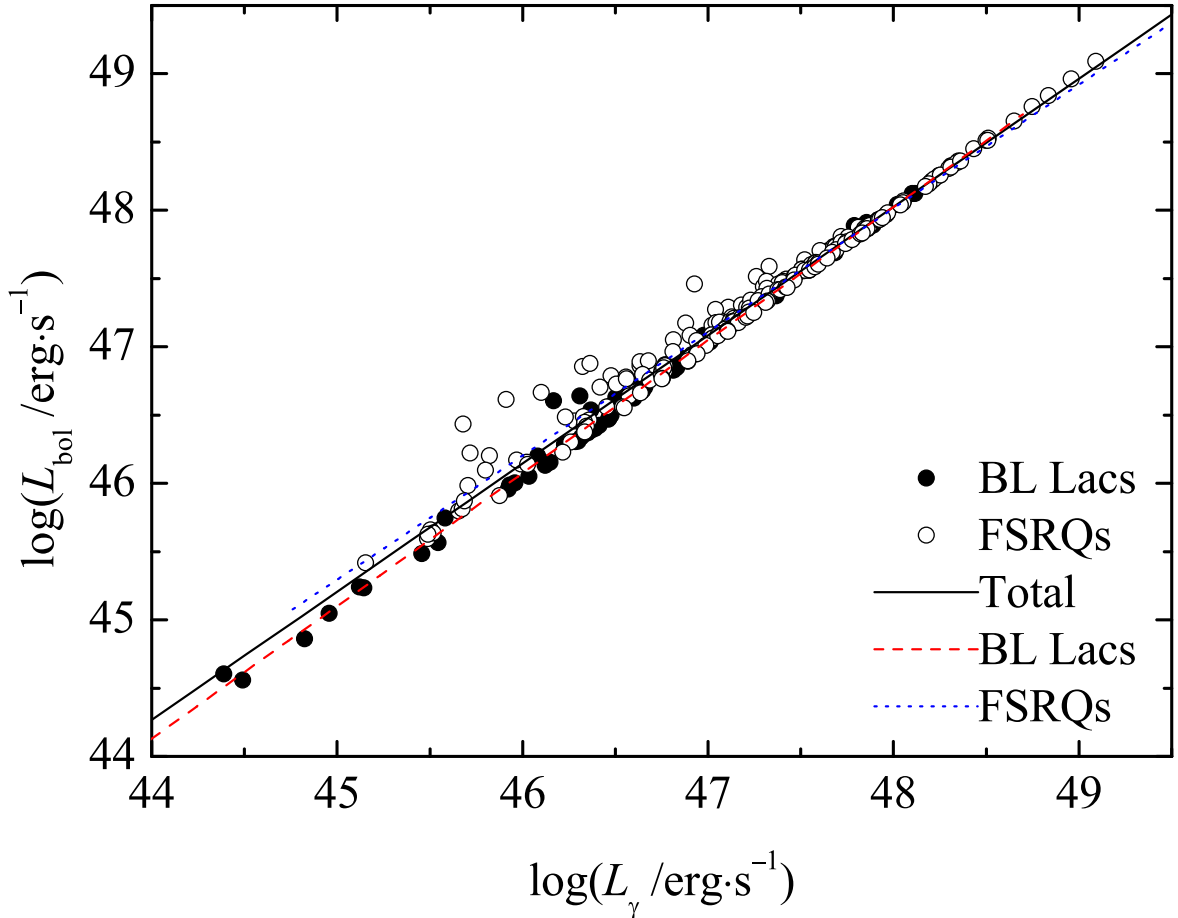


Figure 8. Correlation between the bolometric luminosity ($\log L_{\text{bol}}$) and the γ -ray luminosity ($\log L_{\gamma}$), where filled circles stand for BL Lac objects and open circles for FSRQs.

for BL Lac objects and $\delta = (8.04L_{47})^{\frac{1}{\alpha_{\text{ph}}-1.525}}$ for BCUs, where $L_{47} = L_{\gamma}/(10^{47} \text{ erg s}^{-1})$.

γ -ray Dominance: In this work, the Compton dominance parameter (CDP; $\text{CDP} = \nu_p^{\text{IC}} L_p^{\text{IC}} / \nu_p^{\text{s}} L_p^{\text{s}}$) is calculated and plotted

against the bolometric luminosity, as shown in Figure 7. In the figure, the bolometric luminosity is the sum of the integrated luminosity (L_{syn}) of the synchrotron component and the integrated γ -ray luminosity (L_{γ}) from 1 GeV to 100 GeV.

From Figure 7, which shows 251 sources with $CDP > 1.0$, one can get $\log(CDP) = (0.36 \pm 0.04)\log L_{\text{bol}} - 15.67 \pm 1.94$ with a correlation coefficient $r = 0.487$ and a chance probability of $p < 10^{-4}$. This suggests that sources with higher CDPs tend to have higher bolometric luminosities. We can also say that the inverse Compton emission contributes to the main part of power for bright sources. When the linear regression is performed to the γ -ray luminosity and the bolometric luminosity, it is found that $\log L_{\text{bol}} = (0.94 \pm 0.01)\log L_{\gamma} + 2.94 \pm 0.37$ with $r = 0.991$ and $p < 10^{-4}$ for the whole sample. When BL Lac objects and FSRQs are considered separately, one can get $\log L_{\text{bol}} = (0.97 \pm 0.01)\log L_{\gamma} + 1.29 \pm 0.41$ with $r = 0.997$ and $p < 10^{-4}$ for BL Lac objects and $\log L_{\text{bol}} = (0.91 \pm 0.01)\log L_{\gamma} + 4.50 \pm 0.48$ with $r = 0.989$ and $p < 10^{-4}$ for FSRQs. The corresponding results are shown in Figure 8 and listed in Table 3. So, we can use a γ -ray luminosity as a proxy for the bolometric luminosity for blazars.

The linear regression result indicates that the CDP is correlated with the Doppler factor (δ),

$$\log(CDP) = (0.39 \pm 0.11)\log \delta + 0.96 \pm 0.12,$$

with $r = 0.228$ and $p = 3.33 \times 10^{-4}$ for 244 blazars with $\delta > 1.0$ and $CDP > 1$. The best-fitting result is shown in Figure 7, and indicates that the higher CDP sources tend to have larger Doppler factors.

4. Conclusions

In this work, we compiled a sample of 255 Fermi blazars with available lower-energy monochromatic luminosities at the radio, optical, and X-ray bands; synchrotron peak frequency; synchrotron peak luminosity; integrated synchrotron luminosity; and Doppler factors. Then, we calculated their intrinsic luminosities, intrinsic peak frequency, and CDP and investigated some correlations. Our conclusions are as follows:

(1) On average, BL Lac objects show lower luminosities than FSRQs, $\langle L^{\text{ob}}|_{\text{BL}} \rangle \ll \langle L^{\text{ob}}|_{\text{FSRQ}} \rangle$ at the radio, optical, X-ray, and γ -ray bands for the observed data, but for the intrinsic data, BL Lac objects show almost the same radio luminosity as FSRQs, $\langle L_{\text{R}}^{\text{in}}|_{\text{BL}} \rangle \sim \langle L_{\text{R}}^{\text{in}}|_{\text{FSRQ}} \rangle$, and higher luminosity than FSRQs, $\langle L^{\text{in}}|_{\text{BL}} \rangle \gg \langle L^{\text{in}}|_{\text{FSRQ}} \rangle$ at the optical, X-ray, and γ -ray bands.

(2) We obtained anticorrelations between the luminosity (at radio, X-rays, γ -rays, and peak frequency) and peak frequency. However, those correlations, including that between the optical luminosity and peak frequency for the intrinsic data, are positive, suggesting that the anticorrelations for the observed data may be due to a beaming effect or a selection effect.

(3) The CDP is correlated with both the bolometric luminosity and Doppler factor, implying that the more highly Compton-dominated sources are the more luminous, and this higher luminosity results from Doppler boosting.

(4) The bolometric luminosity can be represented by the γ -ray luminosity for Fermi blazars.

We are happy to thank the anonymous reviewer for the constructive suggestions and comments. The work is partially supported by the National Natural Science Foundation of China (NSFC U2031201, NSFC 11733001, U2031112, NSFC 12133004, NSFC 12103012), Guangdong Major Project of Basic and Applied Basic Research (grant No. 2019B030302001). We also acknowledge the science research grants from the China

Manned Space Project with No. CMS-CSST-2021-A06 and the support of the Astrophysics Key Subjects of Guangdong Province and Guangzhou City. The work is also supported by Guangzhou University (YM2020001).

ORCID iDs

J. H. Yang  <https://orcid.org/0000-0002-4469-9672>
L. X. Zhang  <https://orcid.org/0000-0003-3184-6896>
J. H. Fan  <https://orcid.org/0000-0002-5929-0968>

References

- Abdo, A. A., Ackermann, M., Agudo, I., et al. 2010, *ApJ*, 716, 30
Abdollahi, S., Acero, F., Ackermann, M., et al. 2020, *ApJS*, 247, 33
Acero, F., Ackermann, M., Ajello, M., et al. 2015, *ApJS*, 218, 23
Ajello, M., Angioni, R., Axelsson, M., et al. 2020, *ApJ*, 892, 105
Aller, M. F., Aller, H. D., & Hughes, P. A. 2011, *JApA*, 32, 5
Angel, J. R. P., & Stockman, H. S. 1980, *ARA&A*, 18, 321
Bassani, L., Dean, A. J., & Sembay, S. 1983, *A&A*, 125, 52
Chen, L. 2018, *ApJS*, 235, 39
Chen, Y., Gu, Q., Fan, J., et al. 2021, *ApJ*, 913, 93
Donato, D., Ghisellini, G., Tagliaferri, G., & Fossati, G. 2001, *A&A*, 375, 739
Dondi, L., & Ghisellini, G. 1995, *MNRAS*, 273, 583
Fan, J., Yang, J. H., Zhang, J.-Y., et al. 2013a, *PASJ*, 65, 25
Fan, J. H., Adam, G., Xie, G. Z., et al. 1998, *A&A*, 338, 27
Fan, J.-H., Bastieri, D., Yang, J.-H., et al. 2014, *RAA*, 14, 1135
Fan, J.-H., Huang, Y., He, T.-M., et al. 2009, *PASJ*, 61, 639
Fan, J. H., Kurtanidze, S. O., Liu, Y., et al. 2021, *ApJS*, 253, 10
Fan, J. H., Xie, G. Z., & Bacon, R. 1999, *A&AS*, 136, 13
Fan, J. H., Yang, J. H., Liu, Y., et al. 2016, *ApJS*, 226, 20
Fan, J.-H., Yang, J.-H., Liu, Y., & Zhang, J.-Y. 2013b, *RAA*, 13, 259
Fan, J. H., Yang, J. H., Xiao, H. B., et al. 2017, *ApJL*, 835, L38
Fan, J. H., Yang, J. H., Yuan, Y. H., Wang, J., & Gao, Y. 2012, *ApJ*, 761, 125
Fossati, G., Maraschi, L., Celotti, A., Comastri, A., & Ghisellini, G. 1998, *MNRAS*, 299, 433
Ghisellini, G., Celotti, A., Fossati, G., Maraschi, L., & Comastri, A. 1998, *MNRAS*, 301, 451
Ghisellini, G., Padovani, P., Celotti, A., & Maraschi, L. 1993, *ApJ*, 407, 65
Ghisellini, G., & Tavecchio, F. 2008, *MNRAS*, 386, L28
Ghisellini, G., Tavecchio, F., Maraschi, L., Celotti, A., & Sbarro, T. 2014, *Natur*, 515, 376
Giommi, P., Padovani, P., Polenta, G., et al. 2012a, *MNRAS*, 420, 2899
Giommi, P., Piranomonte, S., Perri, M., & Padovani, P. 2005, *A&A*, 434, 385
Giommi, P., Polenta, G., Lähteenmäki, A., et al. 2012b, *A&A*, 541, A160
Giroletti, M., Pavlidou, V., Reimer, A., et al. 2012, *AdSpR*, 49, 1320
Gupta, A. C. 2020, *Galax*, 8, 64
Hartman, R. C., Bertsch, D. L., Bloom, S. D., et al. 1999, *ApJS*, 123, 79
Homan, D. C., Kadler, M., Kellermann, K. I., et al. 2009, *ApJ*, 706, 1253
Hovatta, T., Lister, M. L., Kovalev, Y. Y., Pushkarev, A. B., & Savolainen, T. 2010, *IJMPD*, 19, 943
Hovatta, T., Valtaoja, E., Tornikoski, M., & Lähteenmäki, A. 2009, *A&A*, 494, 527
Kellermann, K. I., Lister, M. L., Homan, D. C., et al. 2004, *ApJ*, 609, 539
Lähteenmäki, A., & Valtaoja, E. 1999, *ApJ*, 521, 493
Liodakis, I., Hovatta, T., Huppenkothen, D., et al. 2018, *ApJ*, 866, 137
Lister, M. L., Aller, M. F., Aller, H. D., et al. 2015, *ApJL*, 810, L9
Lister, M. L., Aller, M. F., Aller, H. D., et al. 2016, *AJ*, 152, 12
Lister, M. L., Cohen, M. H., Homan, D. C., et al. 2009, *AJ*, 138, 1874
Lister, M. L., & Homan, D. C. 2005, *AJ*, 130, 1389
Lister, M. L., Homan, D. C., Hovatta, T., et al. 2019, *ApJ*, 874, 43
Lu, K.-X., Bai, J.-M., Zhang, Z.-X., et al. 2019, *ApJ*, 887, 135
Mao, P., Urry, C. M., Massaro, F., et al. 2016, *ApJS*, 224, 26
Mattox, J. R., Bertsch, D. L., Chiang, J., et al. 1993, *ApJ*, 410, 609
Nieppola, E., Valtaoja, E., Tornikoski, M., Hovatta, T., & Kotiranta, M. 2008, *A&A*, 488, 867
Padovani, P. 2007, *Ap&SS*, 309, 63
Pei, Z., Fan, J., Bastieri, D., Yang, J., & Xiao, H. 2020a, *SCPMA*, 63, 259511
Pei, Z., Fan, J., Yang, J., & Bastieri, D. 2020b, *PASA*, 37, e043
Piner, B. G., Pushkarev, A. B., Kovalev, Y. Y., et al. 2012, *ApJ*, 758, 84
Raiteri, C. M., Villata, M., Acosta-Pulido, J. A., et al. 2017, *Natur*, 552, 374
Savolainen, T., Homan, D. C., Hovatta, T., et al. 2010, *A&A*, 512, A24
Tripathi, A., Gupta, A. C., Aller, M. F., et al. 2021, *MNRAS*, 501, 5997
Urry, C. M., & Padovani, P. 1995, *PASP*, 107, 803

- Vermeulen, R. C., Readhead, A. C. S., & Backer, D. C. 1994, *ApJL*, 430, L41
- von Montigny, C., Bertsch, D. L., Chiang, J., et al. 1995, *ApJ*, 440, 525
- Wills, B. J., Wills, D., Breger, M., Antonucci, R. R. J., & Barvainis, R. 1992, *ApJ*, 398, 454
- Xiao, H., Fan, J., Rando, R., Zhu, J., & Hu, L. 2020, *AN*, 341, 462
- Xiao, H., Fan, J., Yang, J., et al. 2019, *SCPMA*, 62, 129811
- Yan, D., Wu, Q., Fan, X., Wang, J., & Zhang, L. 2018, *ApJ*, 859, 168
- Yang, J. H., Fan, J. H., Liu, Y., et al. 2017, *Ap&SS*, 362, 219
- Yang, J.-h., Fan, J.-h., Zhang, Y.-l., et al. 2019, *ChA&A*, 43, 23
- Ye, X.-H., & Fan, J.-H. 2021, *PASJ*, 73, 775
- Zensus, J. A., Hough, D. H., & Porcas, R. W. 1987, *Natur*, 325, 36
- Zhang, L., Chen, S., Xiao, H., Cai, J., & Fan, J. 2020, *ApJ*, 897, 10
- Zhang, Y. T., & Fan, J. H. 2019, *AcASn*, 60, 7
- Zheng, Y. G., Kang, S. J., Yang, C. Y., & Bai, J. M. 2020, *MNRAS*, 499, 1188